Comparison of Geometric, Electronic, and Vibrational Properties for Isomers of Small Fullerenes C$_{20}$−C$_{36}$[†]

Edyta Małolepsza and Henryk A. Witek*

Institute of Molecular Science and Department of Applied Chemistry, National Chiao Tung University, Hsinchu, Taiwan

Stephan Irle*

Fukui Institute for Fundamental Chemistry, Kyoto University, Kyoto, Japan

Received: December 12, 2006; In Final Form: February 28, 2007

We employ the self-consistent-charge density-functional tight-binding (SCC−DFTB) method for computing geometric, electronic, and vibrational properties for various topological isomers of small fullerenes. We consider all 35 five- and six-member rings containing isomers of small fullerenes, C$_{20}$, C$_{24}$, C$_{26}$, C$_{28}$, C$_{30}$, C$_{32}$, C$_{34}$, and C$_{36}$, as first part of a larger effort to catalog CC distance distributions, valence CCC angle distributions, electronic densities of states (DOSs), vibrational densities of states (VDOSs), and infrared (IR) and Raman spectra for fullerenes C$_{20}$−C$_{180}$. Common features among the fullerenes are identified and properties characteristic for each specific fullerene isomer are discussed.

1. Introduction

Since the discovery of fullerenes,[1] significant scientific activity has been devoted to investigating their physical and chemical properties.[2] Many studies concerned their geometry,[3] energetic stability,[4−7] spectra,[6,8] and interactions with other molecules. Both theoretical and experimental investigations of fullerene molecules are very challenging. One of the reasons for this situation is the very large number of fullerene geometrical isomers. The number of isomers grows very fast with the number of carbon atoms present in the structure. Small fullerenes have only a few isomers, while larger carbon fullerenes can have an enormous number of structures described by the same chemical formula. The most important isomers of fullerenes are those that contain only five- and six-member rings and obey the "isolated pentagons rule" (IPR).[5,9] This rule states that the structure is energetically stable if the fullerene cage does not contain any adjacent pentagon rings. Such situation minimizes steric strains induced by the presence of five-member rings necessary to introduce curvature in otherwise flat, π-conjugated graphite honeycomb lattice. C$_{60}$ is geometrically the smallest possible fullerene cage able to obey IPR; therefore, all smaller fullerenes fall in the class of the so-called "non-IPR fullerenes".

Large differences in geometry and topology between various fullerene isomers can lead to large differences in their chemical and physical properties.[7] In the present study, we investigate to which extent molecular properties of various isomeric structures of fullerenes are affected by modifying their geometrical and topological parameters. The geometry is usually defined by specifying the point group symmetry of a given isomer. In situations where there exists more than one isomer corresponding to the same symmetry, we enumerate the isomers using subsequent low-case letters. It is very difficult to find a universal way of direct comparison of geometries of different isomers.

In this study, we present distributions of carbon−carbon distances and distributions of angles between two adjacent carbon−carbon bonds. We consider explicitly all five- and six-member-containing isomers of the following fullerenes: C$_{20}$, C$_{24}$, C$_{26}$, C$_{28}$, C$_{30}$, C$_{32}$, C$_{34}$, and C$_{36}$. At present, our consideration is rather theoretical since there is no related experimental data available for any of these species. The available experimental data for small fullerenes concern mostly their synthesis and identification rather than their physical properties. Small fullerene cages are usually unstable and very reactive. It is mainly their anions that were observed experimentally.[10,11] Kietzmann et al.[12] reported quite high stability and abundance of C$_{32}$; other small fullerenes (C$_{36}$, C$_{44}$, and C$_{50}$) were also observed. Some experimental results are also available for C$_{20}$ that was synthesized using standard organic chemistry methods.[13] Piskoti et al. designed experimental conditions to produce C$_{36}$ fullerenes.[14] The existence of some isomers considered in the present study is only hypothetical, but it is entirely possible that they have already been observed in mass spectra and will be characterized experimentally in the future. Therefore, we consider our study of vibrational spectra and electronic structure of small fullerenes as a helpful tool for understanding and predicting their properties. We are planning to perform a comparison of properties of isomers of various fullerenes between C$_{20}$ and C$_{180}$. This paper, which opens the series, gives the results of our simulations for small fullerenes. We are fully aware that more accurate calculations can be performed for these small molecules. Nevertheless, to give a complete treatment of various fullerenes using the SCC−DFTB method, we have decided to present these results.

Theoretical investigation of various physical properties of fullerenes in this study is performed using the self-consistent-charge density-functional tight-binding (SCC−DFTB) method.[15] SCC-DFTB is a semiempirical quantum mechanical technique that allows for fast and qualitative description of large molecular systems. It can be considered as an approximated density

---
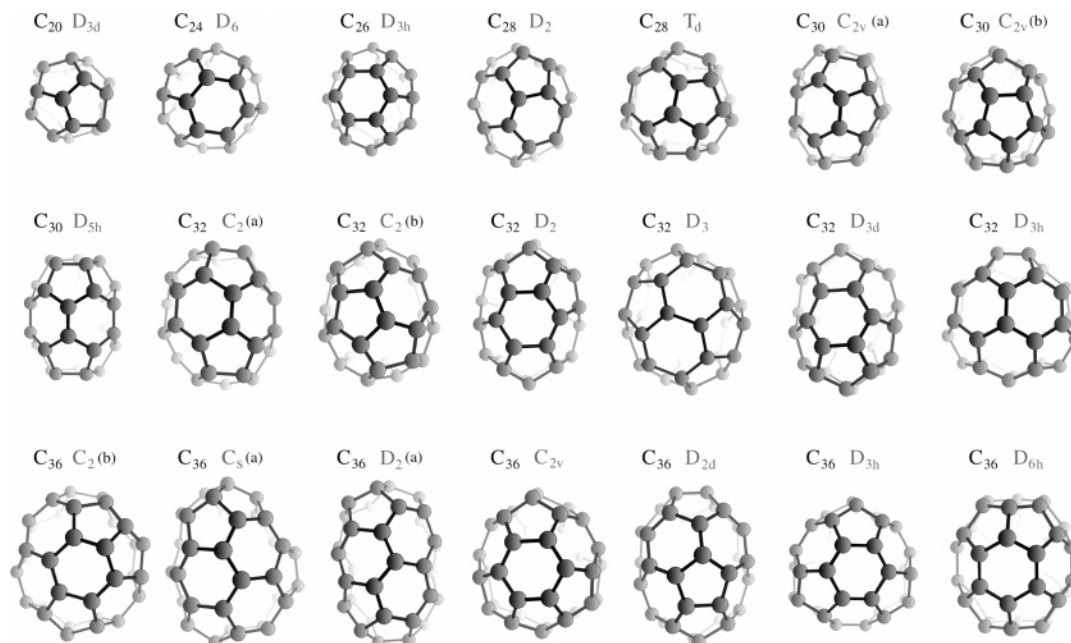
Figure 1. Optimized structures of all five- and six-member ring containing isomers of C_{20}, C_{24}, C_{26}, C_{28}, C_{30}, C_{32}, and seven selected isomers of C_{36}.

functional theory (DFT) that treats explicitly only valence electrons. In SCC−DFTB, molecular electronic density is built from atomic confined densities. The density reorganization, originating from the interactions between atoms, is described effectively via self-consistently determined induced atomic charges. All the approximations introduced in derivation of SCC−DFTB have been carefully designed and tested. The overall accuracy of SCC−DFTB is rather high; reproduced energies, geometries, and vibrational frequencies are comparable to those obtained with DFT.[16] In benchmark studies on geometries and isomer energetics of fullerene cages C_{20} to C_{84}, we found excellent agreement of SCC−DFTB with B3LYP/6-31G(d) results.[17]

The organization of the paper is as follows. The next section contains technical details of our calculations. Section 3 gives a discussion of the calculated properties of all the considered fullerenes isomers: distributions of carbon−carbon distances and valence angles, electronic densities of states (DOS), vibrational densities of states (VDOS), and IR and Raman spectra. In section 4 we present our conclusions.

2. Technical Details

All SCC−DFTB calculations have been performed using a FORTRAN-based DFTB program of Blaudeck and Porezag. For calculating frequencies, we have used analytical Hessian recently implemented in the original code.[18,19] Intensities in vibrational spectra have been computed using numerical derivatives of gradient with respect to the components of external electric field. To obtain intensities in the Raman spectra, we need some parameters describing experimental conditions. We assume that the Raman spectra are generated in temperature 25 °C and the laser frequency is 9398.5 cm^{-1}. Geometries of the fullerene isomers have been taken from the "Fullerene Structure Library".[20] All structures have been optimized with the SCC−DFTB program using a gradient convergence criterion of 10^{-6} atomic units (au). Some of the structures (C_{20} and C_{24}) optimized with SCC−DFTB have lower effective symmetry than those given in the reference.[20] This effect results from the Jahn−Teller distortion of these highly symmetric species. Namely, the

reference I_h symmetry of C_{20} is reduced to the D_{3d} symmetry, and the reference D_{6d} symmetry of C_{24} is reduced to D_6. In both cases, the fractional occupations (4×0.5 for C_{20} and $2 \times 2 \times 1.5$ for C_{24}) of the HOMO orbitals are lifted yielding nice-looking closed shell structures. As in typical Jahn−Teller systems, the resultant structures have lower energy than the nondistorted fullerenes. In one case—the third isomer of C_{30} from the "Fullerene Structure Library"—the SCC−DFTB optimization leads to a structure that has higher effective symmetry than the reference one, i.e., C_{2v} instead of C_s. In our SCC−DFTB calculations, we have employed recently reported new set of Slater-Koster parameters especially reoptimized for reproducing accurate vibrational frequencies.[21] The parameter reoptimization was performed at the level of two-center, core−core repulsive potentials that describe effectively the interaction of chemical cores on two neighbor carbon atoms. Recently, we have used this new repulsive potential for computing IR and Raman spectra of C_{28}, C_{60}, and C_{70}, showing good correspondence of the SCC−DFTB results to high-level DFT calculations and to experimental data.[8] SCC−DFTB is essentially a method designed for the description of closed-shell systems, i.e., systems with double occupation of all occupied molecular orbitals. However, some of the fullerene isomers display very small energy gaps between the HOMO and LUMO orbitals. In some cases, these levels are exactly degenerate owing to a very high point-group symmetry of a given isomer. In other cases, the HOMO and LUMO levels are quasi-degenerate. In both situations we assume automatically fractional occupations of these degenerate or quasi-degenerate orbitals; results presented for these structures should be treated with caution and may require additional justification using a multireference treatment. For high-symmetry structures, we have tried to remove this degeneracy by introducing Jahn−Teller distortions. However, except for C_{20} and C_{24}, optimization of the distorted structures has not produced any additional lowering of energy.

3. Results

We have calculated the following physical properties of the fullerenes isomers: distribution of CC distances, distribution
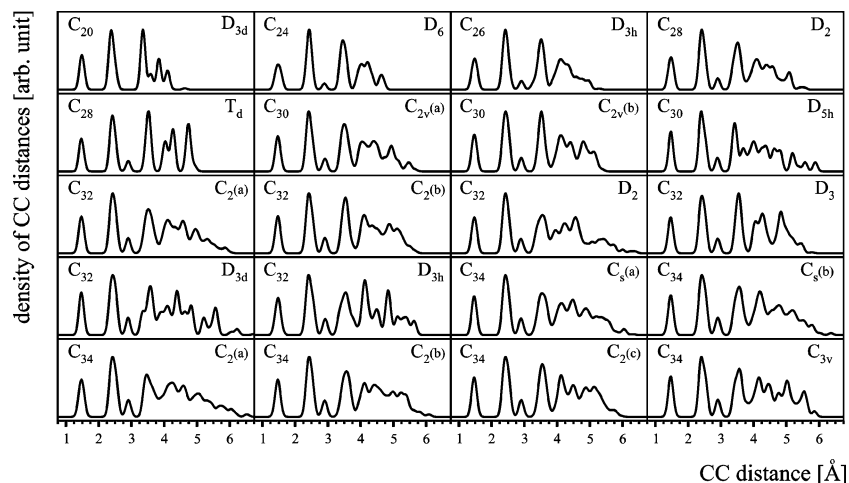
Figure 2. Distribution of CC distances for all studied isomers of small fullerenes: C_{20}, C_{24}, C_{26}, C_{28}, C_{30}, C_{32}, and C_{34}.
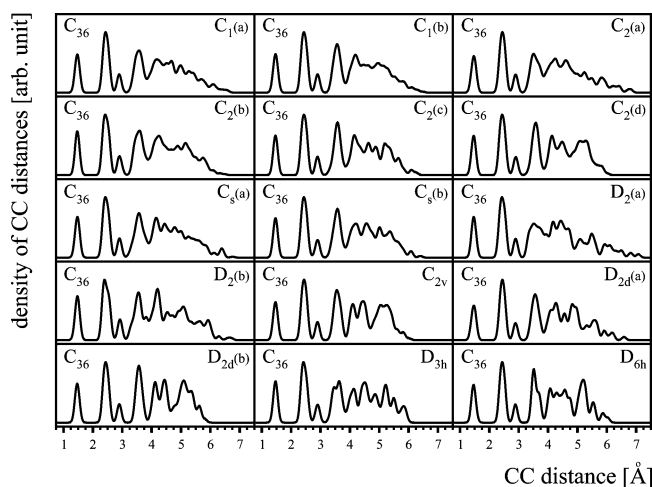
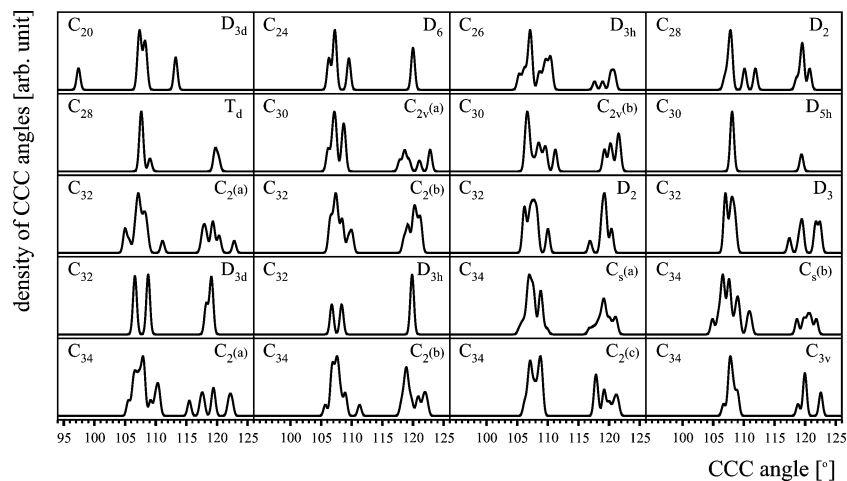**Figure 3.** Distribution of CC distances for all studied isomers of C_{36}.

of valence CCC angles, density of electronic states, density of vibrational states, IR spectra, and Raman spectra. Figure 1 shows optimized structures of all isomers of $C_{20}-C_{32}$ and seven selected isomers of C_{36}. We present these well-known structures to visualize that for small fullerenes change in topology induces large differences in geometry; for larger fullerene cages, this effect is smaller. All optimized molecular structures at the SCC–DFTB level of theory are given in the Supplemental Information. Below we discuss and analyze the obtained results separately for each computed physical property.

3.1. Distribution of CC Distances and CCC Valence Angles. The distribution of CC distances for isomers of $C_{20}-C_{34}$ is shown in Figure 2, while the distribution of CC distances for isomers of C_{36} is presented in Figure 3. All distributions have been normalized in such a way that the height of the highest peak in every graph is equal to one. This presentation of geometries corresponds to pair distribution functions typically reported in solids and liquids; however, we find its use very convenient to discuss the geometrical patterns of the different fullerene isomers on a common footing. As expected, an important feature common to all of the presented plots is the close similarity of the short-range part of the distributions. Since all fullerene cages are comprised of sp^2 carbon atoms, distances corresponding to the first and second neighbors of each carbon atom are nearly identical for all of the studied isomers regardless of its chemical formula and topology. It is interesting to note that also the distances corresponding to the next two neighbors

are very similar for all isomers except for C_{20}. This molecule does not contain any six-member ring in the fullerene cage and the peak corresponding to the diagonal of this ring, and located approximately at 2.9 Å, is missing in the distribution. The long-range part of the distance distributions looks different for every presented isomer. There seems to be no clear correlation between this part of the distribution neither with the number of carbon atoms nor with the point group symmetry of a given fullerene. Therefore, the long-range region can be treated as a unique molecular "fingerprint" useful for experimental differentiation of small carbon fullerenes. Experimentally, curves similar to those shown in Figures 2 and 3 can be obtained from gas-phase electron diffraction or neutron diffraction measurements.[20–22] There is no experimental data available for small fullerenes, but the comparison performed for C_{70} shows that the experimental radial distribution[21] is very similar to that one calculated using the SCC–DFTB method. We would like to stress the importance of this finding and its potential strength in distinguishing various fullerene isomers, although we are aware that gas-phase pair distribution functions of fullerene cages may be difficult to obtain experimentally.

Normalized distributions of CCC valence angles are presented in Figures 4 and 5 for the isomers of $C_{20}-C_{34}$ and C_{36}, respectively. In contrast to the CC distances, we observe some similarity between CCC valence angle distributions for different isomers. All of the analyzed fullerene isomers contain only five- and six-member rings created from sp^2-hybridized carbon atoms. The anticipated values of valence angles should be close to 108° and 120°. We have found that this is indeed the case; however, the deviation from these ideal values is strongly dependent on the topology of the structure. The actual distributions of valence angles presented in Figures 4 and 5 show a small number of rather sharp peaks for highly symmetric structures. For structures with lower symmetry, the number of peaks is larger and their distribution seems to be unique for every isomer, similarly to the long-range part of the CC distance distributions. The angles in the six-member rings can differ from the anticipated value of 120° by up to 7°; similar difference for the five-member ring can be as large as 8°. An interesting anomaly is observed for the smallest studied fullerene, C_{20}, for which significant distortion of the five-member rings owing to a strong Jahn–Teller effect introduces large dispersion of the valence angles. The smallest angle is only 97°; the difference between this and the largest valence angle is 15°.

Figure 4. Distribution of CCC valence bond angles for all studied isomers of small fullerenes: C_{20}, C_{24}, C_{26}, C_{28}, C_{30}, C_{32}, and C_{34}.
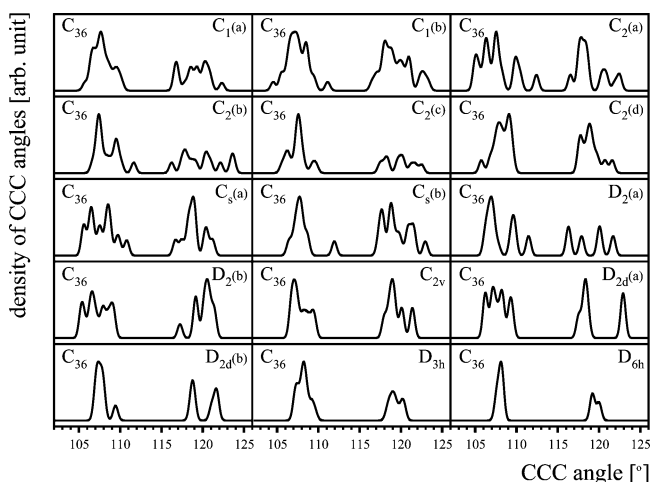

Figure 5. Distribution of CCC valence bond angles for all studied isomers of C_{36}.

In summary, in case of the CC distance distributions, the difference between isomers is visible only for long-range distances. For the valence angles, the plots differ strongly in all the range of values. Even for the isomers characterized by the same chemical formula and identical point group symmetry— for example, the two isomers in symmetry D_2 for C_{36}—the valence angle distributions can be very different. Larger irregularities in the bond angle distribution result from smaller rigidity of the valence angles comparing to the rigidity of the carbon−carbon bonds.
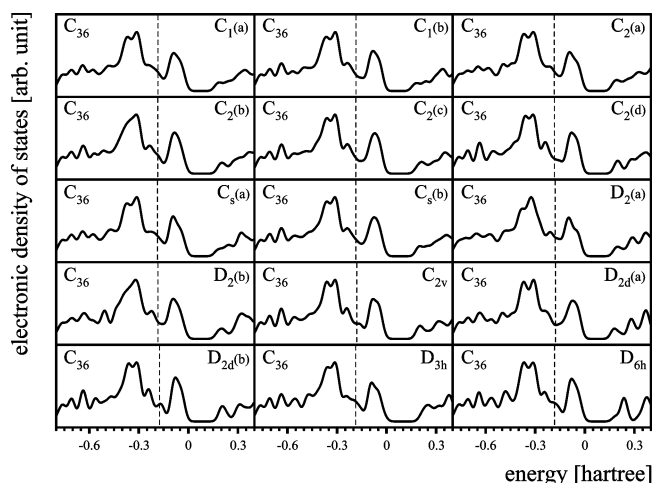
3.2. Electronic Density of States (DOS). Figure 6 presents electronic density of states (DOS) for the isomers of C_{20}–C_{34}, and Figure 7, the electronic densities of states for the isomers of C_{36}. Vertical broken lines at each of the plots show the location of Fermi level that is defined as the averaged value of the HOMO and LUMO energies. The plots have been obtained using a superposition of Gaussian peaks with 0.02 au half-width corresponding to discrete SCC−DFTB, one-electron energy levels. Curves produced in that way differ from usual density-of-states plots obtained from standard momentum space calculations. Still, the presented plots show interesting information concerning the distribution of one-electron levels, as was discussed in our previous work on the DOS of C_{28}, C_{60}, and C_{70}.[8] For all the isomers of C_{34} and C_{36}, there exists large overall similarity of the calculated DOS curves regardless of the fullerene's point group symmetry and topology. This is espe-

cially true for the distribution of one-electron energies located in the vicinity of the Fermi level. The plots corresponding to smaller fullerenes show more structured distributions that are somewhat more characteristic for every isomer. It is interesting to note that the position of the Fermi energy changes only slightly for all the studied isomers; its value is located between −0.1706 and −0.1931 hartree (−4.63 and −5.25 eV). Values of the Fermi energy for all studied fullerenes are collected in Table 1; the fullerenes are ordered according to increasing energy difference between the HOMO and LUMO orbitals. There is no clear correlation between the location of the Fermi level and the symmetry, and the size of a given fullerene. It is interesting to compare these values with Fermi energy of the two most stable fullerenes, C_{60} and C_{70}, that are located at −0.1828 and −0.1827 hartree, respectively.[8] The values of Fermi energies reported in Table 1 are either smaller or larger than the values for C_{60} and C_{70}. It suggests that the value of Fermi energy alone is not a good descriptor of chemical stability of fullerenes. This finding is rather counterintuitive. One can expect that a lower value of Fermi energy for structures containing only carbon atoms should correspond to larger stabilization energy of molecular orbitals. In Table 1 we also compare HOMO−LUMO gaps of the studied structures. Some of the studied structures do not display any gap owing to a fractional occupation of the HOMO orbital. There exist three structures, the D_{3h} isomer of C_{32}, the D_3 isomer of C_{32}, and the $C_{2v}(a)$ isomer of C_{30}, that exhibit particularly large gaps between the HOMO and LUMO energies. These gaps are not as large as those for C_{60} and C_{70} (0.0683 and 0.0591 hartree, respectively),[8] but they are noticeably larger than the gaps for the other studied systems. The large gap of C_{32} relates well with its high abundance in various experiments. Our analysis suggests that the structures observed in experiment can be those of the D_{3h} and D_3 symmetries.

We previously compared the SCC−DFTB electronic densities of states determined for C_{28}, C_{60}, and C_{70} with more accurate calculations performed with DFT.[8] That study showed that SCC−DFTB reproduces with good quality the part of distribution located around and below the Fermi level. The conduction band located above the Fermi energy is not described with sufficient accuracy due to limitations in the SCC−DFTB methodology. SCC−DFTB uses minimal valence basis set and therefore cannot reproduce adequately some of the low-lying one-electron states that often possess very diffuse or Rydberg character. This deficiency of SCC−DFTB may prevent one from
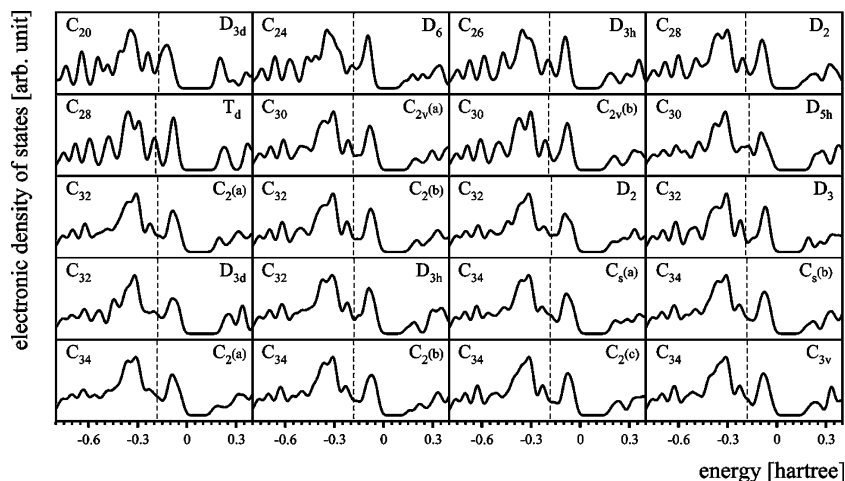
Figure 6. Electronic density of states (DOS) plots for all studied isomers of small fullerenes: C$_{20}$, C$_{24}$, C$_{26}$, C$_{28}$, C$_{30}$, C$_{32}$, and C$_{34}$. Vertical broken line indicates the position of Fermi level.

Figure 7. Electronic density of states (DOS) plots for all studied isomers of C$_{36}$. Vertical broken line indicates the position of Fermi level.

employing this method for calculating higher electronic transitions within the time-dependent linear response theory framework.

3.3. Vibrational Density of States (VDOS). The vibrational density of states (VDOS) is usually used to analyze the distribution of phonons in a crystal. Here, we refer to VDOS as a distribution of vibrational normal modes in a molecule. This type of curves gives information that is complimentary to that obtained from usual vibrational IR and Raman spectra presented below. Vibrational spectra show only the IR or Raman active modes, while the VDOS curves show also the location of silent modes. Silent modes can play an important role in nonradiative intermolecular energy transfer. Detailed knowledge of the distribution of silent modes is also very important for determining molecular vibrational entropy necessary to compute free energy that is a proper descriptor of molecular stability of fullerenes at finite temperatures. We plan to compare the stability of various fullerene isomers at finite temperature in our next study.

The curves of vibrational density of states are presented in Figures 8 and 9 for the isomers of C$_{20}$−C$_{34}$ and C$_{36}$, respectively. The similarity between the curves corresponding to various fullerenes is rather small. However, some of the features—such as the characteristic maximum located at approximately 600

cm^{-1} or a similar range (from 300 cm^{-1} to 1500 cm^{-1}) of the distribution—are present at almost all of the plots. Another characteristic issue of the presented plots is a more distinguished "comb" of individual peaks in VDOSs corresponding to the fullerenes with higher point group symmetry. This effect arises from the increasing degeneracy of vibrational energies. The low-energy part of the distributions looks similar for most of the isomers suggesting that their vibrational entropies are rather similar.

3.4. Vibrational Infrared (IR) Spectra. Figure 10 presents vibrational infrared spectra for isomers of C$_{20}$ through C$_{34}$. Figure 11 presents analogous spectra for isomers of C$_{36}$. The intensities are given in arbitrary units. IR intensities corresponding to fullerenes of different size may differ in magnitude in a large degree. To present all the plots in the same graph, we have adopted various scaling of the vertical axes for various fullerenes. For C$_{20}$ and C$_{24}$, the range of the vertical axis in Figure 10 is [0.00,0.23], and for all the other fullerenes in this figure, it is [0.00,0.09]. The only exception is the D_{3d} isomer of C$_{32}$, for which the vertical axis has the range of [0.00, 0.27]. For all the IR spectra of C$_{36}$ isomers, presented in Figure 11, a uniform scaling of the vertical axis between 0.00 and 0.10 has been used except for the C_2(b) and D_{6h} isomers, for which the maximal value of the vertical axis is 0.20 and 0.25, respectively. The most intensive spectra are those for the D_{3d} isomer of C$_{32}$, the C_2(b) isomer of C$_{36}$, and the D_{6h} isomer of C$_{32}$. The least intensive spectra are usually obtained for low-symmetry structures regardless of their number of atoms. Figures 10 and 11 have been obtained as a superposition of Gaussian peaks with half-width equal to 3 cm^{-1}. The height and location of every peak correspond to the calculated IR intensity and harmonic frequency of each vibrational mode.

The computed IR spectra display a large variety of shapes and patterns. In most of the spectra, the peaks are located in two groups centered around 600 and 1300 cm^{-1}. The spectra corresponding to structures with high symmetry have usually only a few peaks with higher intensities. There is a number of structures, e.g., the C_{2v}(a) isomer of C$_{30}$, the C_2(b) isomer of C$_{34}$, or the C_1(b) and C_{2v} isomers of C$_{36}$, with very low intensities in the spectra. These structures, if observed in a mixture with other isomers, would give too weak signal to be detected; they would be effectively masked by other isomers. It is also very difficult to establish any correspondence between the most intensive peaks in each spectrum and some particular

**TABLE 1: Fermi Energy and HOMO−LUMO Gap for All Studied Isomers of C$_{20}$−C$_{36}$^{a}**

fullerene	symmetry	Fermi energy	HOMO−LUMO gap	fullerene	symmetry	Fermi energy	HOMO−LUMO gap
C$_{60}$	*Ih*	−0.1828	0.0683	C$_{32}$	*D$_{3d}$*	−0.1797	0.0214
C$_{70}$	*D$_{5h}$*	−0.1827	0.0591	C$_{36}$	*C$_s$* (b)	−0.1857	0.0208
C$_{32}$	*D$_{3h}$*	−0.1803	0.0511	C$_{36}$	*D$_{2d}$* (b)	−0.1742	0.0208
C$_{32}$	*D$_3$*	−0.1897	0.0479	C$_{36}$	*C$_1$* (b)	−0.1850	0.0183
C$_{30}$	*C$_{2v}$* (a)	−0.1849	0.0425	C$_{32}$	*C$_2$* (a)	−0.1796	0.0180
C$_{32}$	*C$_2$* (b)	−0.1834	0.0315	C$_{36}$	*C$_2$* (d)	−0.1837	0.0175
C$_{36}$	*D$_{2d}$* (a)	−0.1768	0.0303	C$_{34}$	*C$_s$* (b)	−0.1824	0.0173
C$_{24}$	*D$_6$*	−0.1817	0.0290	C$_{36}$	*C$_1$* (a)	−0.1834	0.0173
C$_{34}$	*C$_2$* (b)	−0.1814	0.0288	C$_{36}$	*C$_2$* (c)	−0.1863	0.0161
C$_{20}$	*D$_{3d}$*	−0.1706	0.0279	C$_{34}$	*C$_2$* (c)	−0.1822	0.0158
C$_{32}$	*D$_2$*	−0.1762	0.0271	C$_{36}$	*D$_{3h}$*	−0.1867	0.0157
C$_{36}$	*D$_2$* (a)	−0.1797	0.0261	C$_{36}$	*C$_2$* (b)	−0.1850	0.0129
C$_{36}$	*C$_{2v}$*	−0.1798	0.0240	C$_{30}$	*C$_{2v}$* (b)	−0.1931	0.0122
C$_{28}$	*D$_2$*	−0.1901	0.0238	C$_{34}$	*C$_s$* (a)	−0.1823	0.0081
C$_{36}$	*C$_2$* (a)	−0.1847	0.0236	C$_{36}$	*D$_{6h}$*	−0.1829	0.0077
C$_{36}$	*C$_s$* (a)	−0.1863	0.0219	C$_{34}$	*C$_{3v}$*	−0.1808	none (2/2)
C$_{36}$	*D$_2$* (b)	−0.1840	0.0219	C$_{30}$	*D$_{5h}$*	−0.1754	none (2/2)
C$_{34}$	*C$_2$* (a)	−0.1813	0.0217	C$_{28}$	*T$_d$*	−0.1897	none (4/3)
C$_{26}$	*D$_{3h}$*	−0.1857	0.0214				

^{a} All values are given in hartree. Fermi energy and HOMO−LUMO gap of C$_{60}$ and C$_{70}$ are also given for comparison. The structures are ordered according to increasing HOMO−LUMO energy differences. For structures with degenerate HOMO and LUMO orbitals, additional information is given describing their degeneracy pattern; e.g., (4/3) denotes four electrons distributed among three degenerate orbitals.
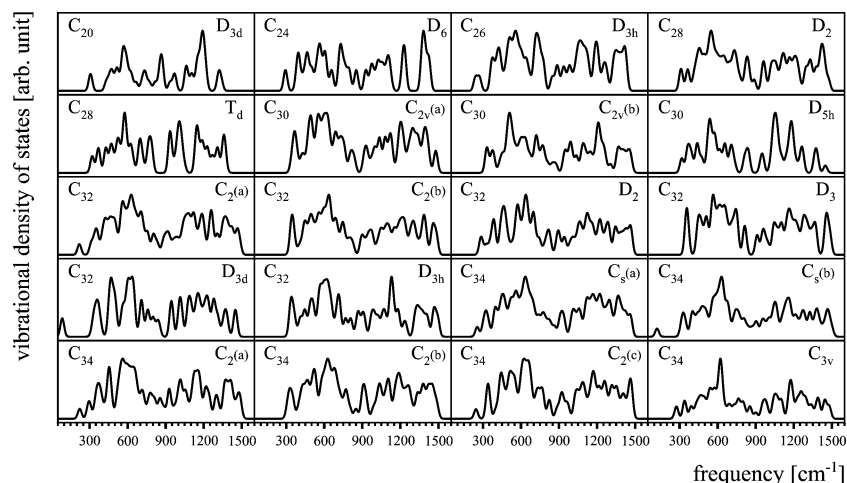

Figure 8. Vibrational density of states (VDOS) plots for all studied isomers of small fullerenes: C$_{20}$, C$_{24}$, C$_{26}$, C$_{28}$, C$_{30}$, C$_{32}$, and C$_{34}$.
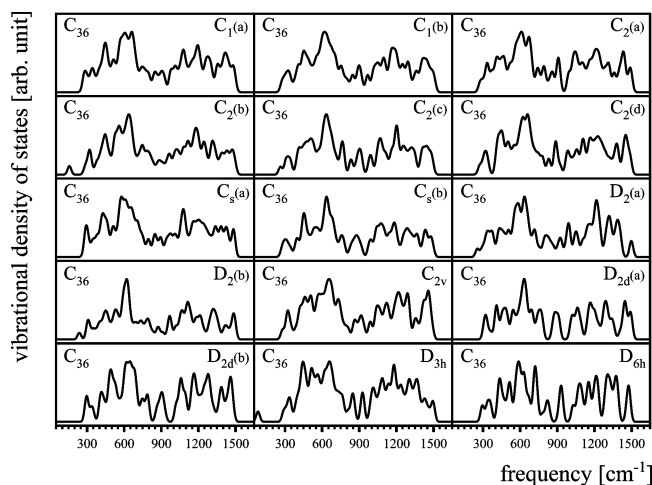
Figure 9. Vibrational density of states (VDOS) plots for all studied isomers of C$_{36}$.

group of vibrational modes responsible for their appearance. We have analyzed the origin of some of the most intensive peaks in spectra presented in Figures 10 and 11. For C$_{20}$, the two most

intensive peaks, located at approximately 440 and 1150 cm^{-1}, correspond respectively to the antisymmetric displacement along the C$_3$ axis of the two carbon atoms that are located on the axis (terminal atoms), and the antisymmetric displacement along the C$_3$ axis of the six carbon atoms that are the first neighbors of the terminal atoms. For C$_{24}$, the most intensive peak originates from the vibrational mode corresponding to a collective symmetric breathing-like displacement of all equatorial carbon atoms. The direction of the breathing displacement (in or out) is alternating for every second atom in the equatorial belt. (We define the equatorial belt as a set of atoms located close to the plane perpendicular to the C$_6$ axis and crossing the center of mass.) For the T$_d$ isomer of C$_{28}$, the most intensive peak, located at approximately 800 cm^{-1}, corresponds to the breathing mode of the six-member rings. For the C$_2$(b) isomer of C$_{32}$, the most intensive peak originates from the stretching of the CC bond connecting two five-members rings. For the C$_{3v}$ isomer of C$_{34}$, the most intensive peak is related to the collective displacement of carbon atoms located in the equatorial belt of the fullerene. The most intensive peak in the spectrum of the D$_{2d}$(b) isomer of C$_{36}$ fullerene originates from the antisymmetric out-of-plane displacement of two carbon atoms located in the bond connect-
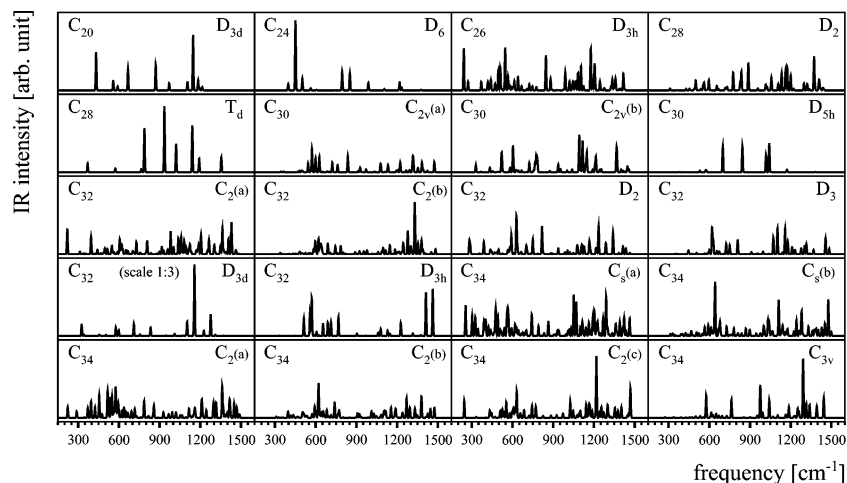
Figure 10. Calculated IR spectra for all studied isomers of small fullerenes: C$_{20}$, C$_{24}$, C$_{26}$, C$_{28}$, C$_{30}$, C$_{32}$, and C$_{34}$. Intensity axis is identical for all the presented plots except for C$_{20}$, C$_{24}$, and the D_{3d} isomer of C$_{32}$; for details, see text.
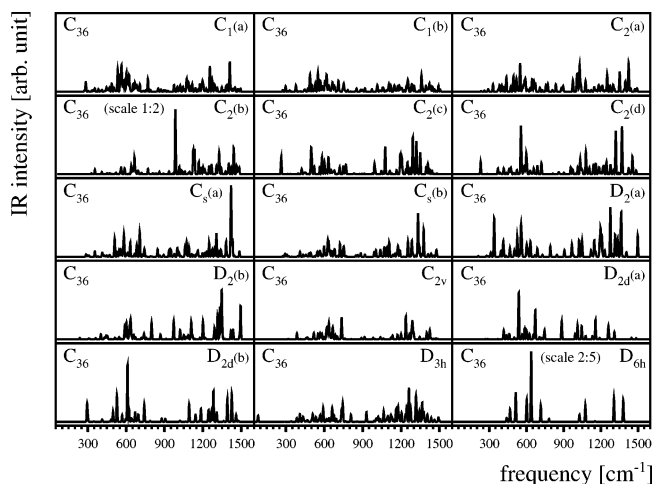
Figure 11. Calculated IR spectra for all studied isomers of C$_{36}$. Intensity axis is identical for all the presented plots except for the C_2-(b) and D_{6h} isomers; for details, see text.

ing two adjacent six-member rings. For the C_s(a) isomer of C$_{36}$, the highest peak is related to a in-plane displacement of the bond connecting two adjacent five-member rings; the displacement is perpendicular to the axis of the bond. The most intensive peak in the spectrum of the D_{6h} isomer of C$_{36}$ corresponds to a collective, chairlike deformation of the benzene rings located in the equatorial belt of the molecule.

We have given this rather long description of vibrational modes, responsible for producing most intensive peaks in the IR spectra reported here, to visualize that there is practically no common mechanism responsible for producing intensive peaks in the IR spectra of small fullerene. Only in three cases— C$_{24}$, the C_{3v} isomer of C$_{34}$, and the D_{6h} isomer of C$_{36}$—can a collective vibrational mode of carbon atoms located close to the equatorial plane of the molecule result in a high intensity of the corresponding peak. However, the harmonic frequencies corresponding to these modes are very different showing that the similarity is rather accidental. Summarizing, we can say that the IR spectra of small fullerenes are very different from each other and can be treated as a "fingerprint" of every structure.

3.5. Vibrational Raman spectra. Calculated Raman spectra of isomers of C$_{20}$–C$_{34}$ are presented in Figure 12. Corresponding spectra of isomers of C$_{36}$ are presented in Figure 13. The curves have been obtained as a superposition of Gaussian peaks with

half-width of 5 cm^{-1}. The intensity of every peak is calculated using the procedure described in ref 19. The calculated Raman plots contain smaller number of peaks than the corresponding IR spectra. The reason for this situation is larger relative difference in Raman activities for different vibrational modes. We find also closer similarity between all the calculated Raman spectra than between the IR spectra discussed above, which is partially a consequence of the small number of Raman active modes. There are two features present in all of the spectra. The first feature is a group of peaks located at approximately 300 cm^{-1}. These peaks correspond to various axial deformations of the fullerene cage, e.g., flattening or elongation along some molecular axis.[25] This is usually the most intensive group of peaks in the spectrum. The second feature is observable at approximately 600 cm^{-1} and is related to a fully symmetric radial breathing mode of the fullerene cage.[26] In some cases, e.g., the D_2 isomer of C$_{32}$ or C_2(b) isomer of C$_{36}$, the breathing mode couples with other vibrational modes that have similar energy yielding a group of peaks of similar intensity and character. The position of the peaks corresponding to the axial deformations of the fullerene cage does not depend strongly on the size or symmetry of the isomer. On the other hand, we have found that the position of the radial breathing mode depends very strongly on the size of the fullerene. For small fullerenes, its vibrational frequency is relatively large (817 cm^{-1} for C$_{20}$). For larger fullerenes, its value is smaller, and for C$_{36}$ it is lying between 596 and 621 cm^{-1}. The corresponding values of the radial breathing modes of C$_{60}$ and C$_{70}$ are 490 cm^{-1} and 458 cm^{-1}, respectively.[8] Both of these modes are observable in the Raman spectra of these molecules. Dependence of the frequency of the radial breathing mode on the number of atoms in a fullerene is a very interesting finding. It has been previously observed experimentally[26] by Eisler and co-workers for larger fullerenes. It can be compared in nature to very well-known relationship between the diameter of a carbon nanotube and the location of its breathing mode in Raman spectrum. The presented data suggest that a very similar relationship can be inferred also for fullerenes. We plan to investigate this relationship in details in our next study using a larger group of fullerenes.
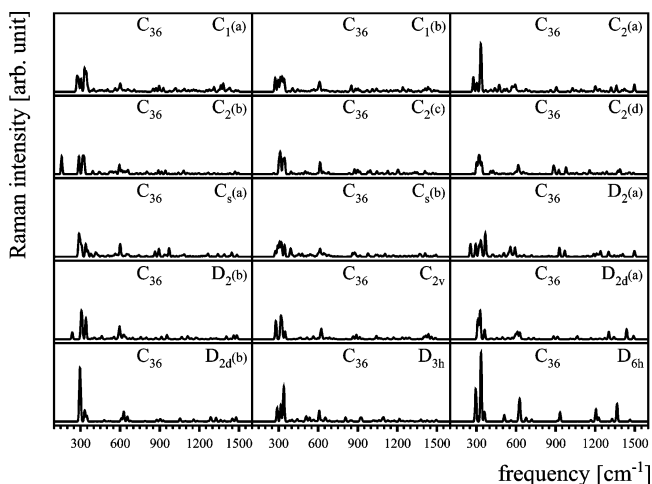
4. Conclusions

We have calculated the following physical properties of C$_{20}$, C$_{24}$, C$_{26}$, C$_{28}$, C$_{30}$, C$_{32}$, C$_{34}$, and C$_{36}$ fullerene isomers:
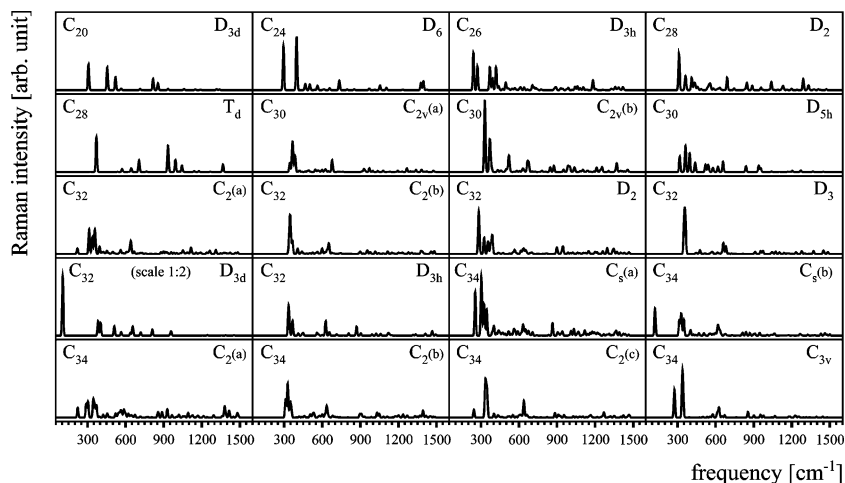
Figure 12. Calculated Raman spectra for all studied isomers of small fullerenes: C_{20}, C_{24}, C_{26}, C_{28}, C_{30}, C_{32}, and C_{34}. All plots have similar scaling of the intensity axes except for the D_{3d} isomer of C_{32}.

Figure 13. Calculated Raman spectra for all studied isomers of C_{36}. All plots have identical scaling of the intensity axes.

distribution of CC distances, distribution of valence CCC angles, density of electronic states (DOS), density of vibrational states (VDOS), and IR and Raman spectra. The different physical properties exhibit different degrees of structural dependence in their appearance, and we are able to pinpoint some of them as useful criteria for structural characterization of small fullerene cages. They are:

1) C−C distance distributions (pair distribution functions), which exhibit a fingerprint area beyond the second bond partner for each isomer;

2) IR spectra which vary greatly from species to species in overall appearance and features.

Compared to these very characteristic quantities for each fullerene isomer, the valence CCC angle distributions, DOSs, VDOSs, and Raman spectra are much less sensitive to the actual molecular geometry, and exhibit rather common features among all the small fullerenes:

a) angle distributions are centered around 108° and 120° and show little variation except for highly strained cases such as C_{20}, but the largest deviation is only found to be 8°, with highly symmetric structures showing slightly fewer features;

b) DOSs are typically finite around the Fermi energy, indicating the close vicinity of HOMO and LUMO orbitals, with a large number of states appearing below the Fermi level, and a characteristic, rather sharp peak between −0.3 and 0.0 hartree;

c) VDOSs show a characteristic maximum located at approximately 600 cm^{-1} in all cases, owing to a large variety of different cage vibrations;

d) Raman spectra have typically two highly active groups of modes around 300 and 600 cm^{-1} corresponding to various cage deformations: ellipsoidal structural deformations at lower frequencies and radial breathing mode at higher frequencies.

The identified common features should be useful in discerning between fullerene cages and other carbon nanostructures while the more characteristic properties under criteria 1 and 2 can give detailed information on the specific type of isomer. We have compiled this data as the first part of a larger, systematic study of the aforementioned physical properties of fullerene isomers between C_{20} and C_{180} with the hope to assist experimentalists in the characterization and identification of fullerene isomers.

Supporting Information Available: Cartesian coordinates of fullerene isomers C_{20}, C_{24}, C_{26}, C_{28}, C_{30}, C_{32}, C_{34}, and C_{36} optimized at the SCC−DFTB level of theory are given as supplemental information. This material is available free of charge via the Internet at http://pubs.acs.org.

References and Notes

(1) Kroto, H. W.; Heath, J. R.; O'Brien, S. C.; Curl, R. F.; Smalley, R. E. *Nature* **1985**, *318*, 162.

(2) Osawa, E. Presentation at the International Fullerenes Workshop, Dordrecht, The Netherlands, 2001. Unpublished work, 2001.

(3) Fowler, P. W.; Manopoulous, D. E. *An Atlas of Fullerenes*; Oxford University Press: Oxford, UK, 1995.

(4) Fowler, P. W. *Chem. Phys. Lett.* **1986**, *131*, 444. Martin, J. M. L. *Chem. Phys. Lett.* **1996**, *255*, 1; Kent, P. R. C.; Towler, M. D.; Needs, R. J.; Rajagopal, G. *Phys. Rev. B* **2000**, *62*, 15394.

(5) Kroto, H. W. *Nature* **1987**, *329*, 529.

(6) Martin, J. M. L.; El-Yazal, J.; Francois, J. P. *Chem. Phys. Lett.* **1996**, *255*, 7; Chen, Z.; Heine, T.; Jiao, H.; Hirsch, A.; Thiel, W.; Schleyer, P. v. R. *Chem. Eur. J.* **2003**, *9*, 1.

(7) Lu, X.; Chen, Z. *Chem. Rev.* **2005**, *105*, 3643.

(8) Witek, H. A.; Irle, S.; Zheng, G.; de Jong, W. A.; Morokuma, K. *J. Chem. Phys.* **2006**, *125*, 214706.

(9) Fowler, P. W.; Batten, R. C.; Manopoulous, D. E. *J. Chem. Soc., Faraday Trans.* **1991**, *87*, 3103; Fowler, P. W.; Manopoulous, D. E.; Ryan, R. P. *Carbon* **1992**, *30*, 1235.

(10) von Helden, G.; Hsu, M. T.; Gotts, N. G.; Kemper, P. R.; Bowers, M. T. *Chem. Phys. Lett.* **1993**, *204*, 15.

(11) Handschuh, J. H.; Ganteför, G.; Kessler, B.; Bechthold, P. S.; Eberhardt, W. *Phys. Rev. Lett.* **1995**, *74*, 1095.

(12) Kietzmann, H.; Rochow, R.; Ganteför, G.; Eberhardt, W.; Vietze, K.; Seifert, G.; Fowler, P. W. *Phys. Rev. Lett.* **1998**, *81*, 5378.

(13) Sackers, E.; Osswald, T.; Weber, K.; Keller, M.; Hunkler, D.; Woerth, J.; Knothe, L.; Prinzbach, H. *Chem. Eur. J.* **2006**, *12*, 6242.

(14) Piskoti, C.; Yarger, J.; Zettl, A. *Nature* **1998**, *393*, 771.

(15) Porezag, D.; Frauenheim, T.; Köhler, T.; Seifert, G.; Kaschner, R. *Phys. Rev. B* **1995**, *51*, 12947. Elstner, M.; Porezag, D.; Jungnickel, G.; Elsner, J.; Haugk, M.; Frauenheim, T.; Suhai, S.; Seifert, G. *Phys. Rev. B* **1998**, *58*, 7260.

(16) Frauenheim, T.; Seifert, G.; Elsterner, M.; Hajnal, Z.; Jungnickel, G.; Porezag, D.; Suhai, S.; Scholz, R. *Phys. Status Solidi, B* **2000**, *217*, 41.

(17) Zheng, G.; Irle, S.; Morokuma, K. *Chem. Phys. Lett.* **2005**, *412*, 210.

(18) Witek, H. A.; Irle, S.; Morokuma, K. *J. Chem. Phys.* **2004**, *121*, 5163; Witek, H. A.; Morokuma, K.; Stradomska, A. *J. Theor. Comput. Chem.* **2005**, *4*, 639.

(19) Witek, H. A.; Morokuma, K.; Stradomska, A. *J. Chem. Phys.* **2004**, *121*, 5171.

(20) Yoshida, M. http://www.cochem2.tutkie.tut.ac.jp/Fuller/fsl/fsl.html (accessed 2006).

(21) Malolepsza, E.; Witek, H. A.; Morokuma, K. *Chem. Phys. Lett.* **2005**, *412*, 237.

(22) Hedberg, K.; Hedberg, L.; Bethune, D. S.; Brown, C. A.; Dorn, H. C.; Johnson, R. D.; de Vries, M. *Science* **1991**, *254*, 410.

(23) Hedberg, K.; Hedberg, L.; Bühl, M.; Bethune, D. S.; Brown, C. A.; Johnson, R. D. *J. Am. Chem. Soc.* **1997**, *119*, 5314.

(24) Nikolaev, A. V.; Dennis, T. J. S.; Prassides, K.; Soper, A. K. *Chem. Phys. Lett.* **1994**, *223*, 143.

(25) Eisler, H.-J.; Hennrich, F. H.; Gilb, S.; Kappes, M. M. *J. Phys. Chem. A* **2000**, *104*, 1769.

(26) Eisler, H.-J.; Gilb, S.; Hennrich, F. H.; Kappes, M. M. *J. Phys. Chem. A* **2000**, *104*, 1762.